LETTERS
PUBLISHED ONLINE: 3 JULY 2017 | DOI: 10.1038/NPHYS4189
nature physics

Testing sub-gravitational forces on atoms from a miniature in-vacuum source mass

Matt Jaffe[1†], Philipp Haslinger[1†], Victoria Xu[1], Paul Hamilton[2], Amol Upadhye[3], Benjamin Elder[4], Justin Khoury[4] and Holger Müller[1,5*]

Traditional gravity measurements use bulk masses to both source and probe gravitational fields[1]. Matter-wave interferometers enable the use of probe masses as small as neutrons[2], atoms[3] and molecular clusters[4], but still require fields generated by masses ranging from hundreds of kilograms[5,6] to the entire Earth. Shrinking the sources would enable versatile configurations, improve positioning accuracy, enable tests for beyond-standard-model ('fifth') forces, and allow observation of non-classical effects of gravity. Here we detect the gravitational force between freely falling caesium atoms and an in-vacuum, miniature (centimetre-sized, 0.19 kg) source mass using atom interferometry. Sensitivity down to gravitational strength forces accesses the natural scale[7] for a wide class of cosmologically motivated scalar field models[8,9] of modified gravity and dark energy. We improve the limits on two such models, chameleons[9] and symmetrons[10,11], by over two orders of magnitude. We expect further tests of dark energy theories, and measurements of Newton's gravitational constant and the gravitational Aharonov–Bohm effect[12].

Light-pulse atom interferometry[3] is based on the wave–particle duality of quantum mechanics and transduces the acceleration experienced by atoms into a phase difference between interfering atomic matter waves. In our set-up, caesium atoms are laser-cooled and launched[13] upwards into free fall. Pulses from counter-propagating laser beams transfer them from their initial quantum state $|a\rangle$ to another state $|b\rangle$. Each atom absorbs one photon, having a momentum $\hbar k_1$, from the first beam while simultaneously being stimulated to emit another photon into the second beam, gaining additional momentum $\hbar k_2$. This results in a total momentum change of $\hbar k_{\mathrm{eff}}$, where $k_{\mathrm{eff}} = k_1 + k_2$. The first interferometer pulse has a duration such that the transfer takes place with 50% probability. It acts as a coherent beam splitter for matter waves, placing the atom into a superposition of the initial state $|a, p_0\rangle$ with momentum p_0 and the state $|b, p_0 + \hbar k_{\mathrm{eff}}\rangle$. The two states separate spatially. After a pulse separation time T, a second laser pulse transfers the states $|a, p_0\rangle \rightarrow |b, p_0 + \hbar k_{\mathrm{eff}}\rangle$ and $|b, p_0 + \hbar k_{\mathrm{eff}}\rangle \rightarrow |a, p_0\rangle$, thus inverting the relative motion. After another interval T, a third pulse acts as a final beam splitter which combines the partial matter waves (Fig. 1). When combined, the matter waves add constructively or destructively, depending on their phase difference $\Delta\phi$, giving a probability $P \sim \cos^2(\Delta\phi/2)$ of finding the atom in the quantum state $|a\rangle$. The probability and thus the phase difference is found by measuring the population ratio of states $|a\rangle$ and $|b\rangle$ when many atoms undergo this process simultaneously. In the simplest case, $\Delta\phi = k_{\mathrm{eff}} a T^2$, where a is the total acceleration experienced by the atoms. Using $k_{\mathrm{eff}} \sim 10^7\,\mathrm{m}^{-1}$, large atom samples for sufficient phase resolution, and T of up to 1.15 s (ref. 14) creates an enormous lever arm by which even small changes of a generate measurable phase changes.

Unfortunately, this lever arm is significantly shortened when it comes to measuring the gravitational force created by a small mass M. The useful free-fall time, distance between the atoms and the source mass, and the dimensions of the atom cloud are all constrained because atoms far away from the source see a reduced gravitational potential. Accordingly, the most sensitive atom interferometers[15,16] use the entire Earth as a source mass. Measurements using small source masses have not been previously demonstrated, but could be useful to explore new regimes[12,17].

Testing gravity in new ways may help to answer pressing questions. Cosmological measurements[18,19] have firmly established that the universe is expanding at an accelerating rate which is consistent with dark energy permeating all of space. The observed dark energy density $\Lambda_0^4 \approx (2.4\,\mathrm{meV})^4$ is tens of orders of magnitude smaller than expected from the vacuum energy of quantum field theories. This chasm, the 'cosmological-constant problem,' probably requires new fields for its resolution. By Weinberg's no-go theorem[20], however, even such new fields cannot solve the problem unless they are dynamic, not in equilibrium. A new field must therefore be light if it is to address the cosmological-constant problem, ($m \leq H_0$ where $H_0 \sim 10^{-33}$ eV is the Hubble constant) so as to remain in non-equilibrium today, 10^{10} years after the Big Bang. Such a light field, however, should mediate a long-range interaction, in disagreement with precision tests of gravity. Over the past decade, this has motivated a family of theories that predict significant deviations from general relativity only in the ultraweak-field regime[20], where a force of gravitational strength or larger is suppressed further by 'screening' as a function of the environment. Existing theories do not solve the cosmological-constant problem, but screening is probably a key ingredient of any future solution. Experimental tests of gravity have focused on the short-distance regime, the post-Newtonian regime or the strong field regime[21], leaving the ultraweak-field regime largely untested.

Screening arises when coupling between the field and matter hides effects of the field (such as a new force) in high-density regions like Earth. In contrast, the field is unsuppressed and most potent in low-density regions like the cosmos. Such fields can enact important astrophysical effects while remaining hidden from laboratory and solar system tests.

[1]Department of Physics, 366 Le Conte Hall MS 7300, University of California, Berkeley, California 94720, USA. [2]Department of Physics and Astronomy, University of California, Los Angeles, California 90095, USA. [3]Department of Physics, University of Wisconsin-Madison, Madison, Wisconsin 53706, USA. [4]Center for Particle Cosmology, Department of Physics and Astronomy, University of Pennsylvania, Philadelphia, Pennsylvania 19104, USA. [5]Lawrence Berkeley National Laboratory, One Cyclotron Road, Berkeley, California 94720, USA. [†]These authors contributed equally to this work.
*e-mail: hm@berkeley.edu

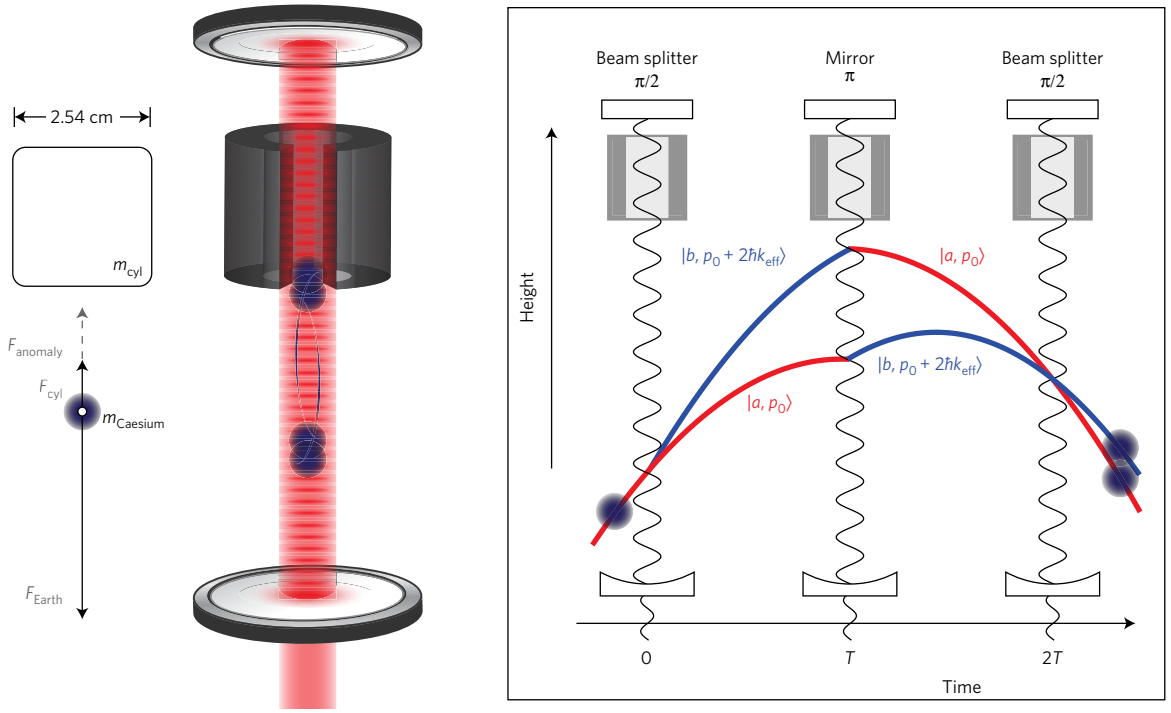

Figure 1 | Cavity matter-wave interferometry. Left: experimental set-up. The acceleration a_{cyl} of caesium atoms towards a cylindrical tungsten source mass suspended in ultrahigh vacuum is measured. The cylinder has mass $m_{cyl} = 0.19$ kg, height h and diameter $d = h = 2.54$ cm. The axial through-hole has radius 0.5 cm, and the slot has width 0.5 cm. Making a differential measurement isolates the effect of any interactions sourced by the tungsten mass. Right: Mach–Zehnder interferometer based on Raman transitions in an optical cavity. Three laser pulses manipulate the caesium atoms during free fall. The pulses split the atomic wavepacket along two different trajectories, reflect the two trajectories near their apex, and then recombine and interfere the matter waves to measure the phase difference accumulated between the two paths during the interferometer time of $2T = 110$ ms. We obtain a measurement of the acceleration experienced by the caesium atoms ensemble-averaged over $\sim 10^5$ atoms.

The ultraweak fields φ can be characterized by their mass $m(\varphi)$ and coupling to normal matter $\beta(\varphi)$, which may both be functions of the field itself. The acceleration of an object

$$a = -\frac{\beta(\varphi)}{M_{Pl}} \lambda_a \nabla\varphi \tag{1}$$

(in our case, an atom) caused by the field is highly sensitive to the surrounding matter geometry[22]. Here, $M_{Pl} = (\hbar c/8\pi G)^{1/2} \approx 2.4 \times 10^{18}$ GeV is the reduced Planck mass, and $0 \leq \lambda_a \leq 1$ is a screening function that depends on m, β and the object's mass and size. Moreover, $\lambda_a \to 1$ for a small and light test particle but $\lambda_a \ll 1$ for macroscopic objects, where only a thin, outermost layer interacts with the field. An atom in ultrahigh vacuum with a local miniature source mass minimizes screening and is well-suited as a test mass for such theories[8]. Prime examples of such scalar fields are chameleons and symmetrons.

A chameleon scalar field[23,24] is characterized by an effective potential density

$$V_{eff}(\varphi) = V(\varphi) + V_{int}(\varphi) \tag{2}$$

The self-interaction

$$V(\varphi) = \Lambda^4 + \frac{\Lambda^{4+n}}{\varphi^n} \tag{3}$$

is characterized by an energy scale Λ, which must be close to the cosmological-constant scale, $\Lambda \simeq \Lambda_0 = 2.4$ meV, if the chameleon is to drive cosmic acceleration. The interaction with matter of density ρ_m

$$V_{int} = \rho_m \varphi / M \tag{4}$$

is characterized by an energy scale M, which is expected to be below the Planck mass. The chameleon profile due to an arbitrary static distribution of matter $\rho_m(\mathbf{x})$ is obtained by solving the nonlinear Poisson equation:

$$\nabla^2\varphi = \partial V_{eff}/\partial\varphi \tag{5}$$

Deep inside a large, dense object, $\nabla^2\varphi \simeq 0$ and φ rapidly approaches a negligible value that minimizes $V_{eff}(\varphi)$. Thus, the bulk of such an object is largely decoupled from the field, except for a thin outer shell, leading to screening. For general $\rho_m(\mathbf{x})$, we must resort to numerical integration[22]. Given the resulting field profile $\varphi(\mathbf{x})$, the chameleon-mediated acceleration on an atom is given by equation (1) with $\beta_{cham} = M_{Pl}/M$.

A symmetron scalar field[25,26] has an effective potential symmetric under $\varphi \to -\varphi$. The simplest models have a Higgs-like quartic self-interaction

$$V(\varphi) = \frac{\lambda}{4!}\varphi^4 - \frac{\mu^2}{2}\varphi^2 \tag{6}$$

in which λ is the self-coupling, and μ is the bare potential mass scale. The field couples to matter through an explicitly density-dependent mass term,

$$V_{int}(\varphi) = \frac{\rho_m}{2M_S^2}\varphi^2 \tag{7}$$

The coupling is again characterized by an energy scale M_S. We focus here on $1\,\text{MeV} < M_S < 1\,\text{TeV}$, approximately the regime in which the fifth force is screened in a typical laboratory apparatus. The acceleration equation (1) in a constant-density region is roughly characterized by $\beta_{sym}(\varphi) = \varphi M_{Pl}/M_S^2$. The field φ, and thus the coupling β_{sym}, is zero in high-density regions and nonzero at low

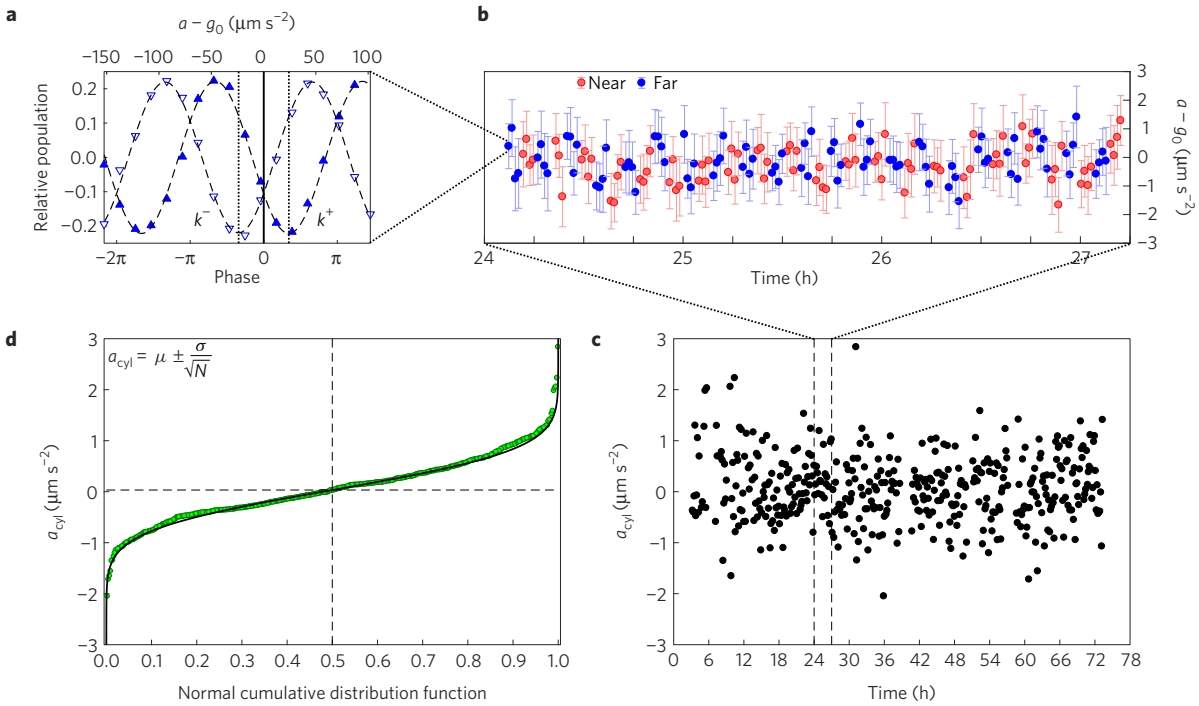

Figure 2 | Experimental data. A differential measurement is performed by toggling the source mass between a near and far position. **a**, Two interferometer fringes, taken for the wavevector direction, up (k^+) and down (k^-) (see Methods). Combining these two measurements gives one data point out of 3,215 taken over 68 h. **b**, A 3-hour section of data. Four measurements are taken at each source mass position, which are then averaged. Blue points indicate that the source mass is in the far position; red points indicate the near position. An overall offset g_0 is subtracted for clarity. The difference between subsequent measurements after toggling the source mass position gives one measurement of a_{cyl}. Error bars represent 1-σ standard deviation (statistical). **c**, A single determination of a_{cyl} takes ∼500 s. The full dataset (one of three) is shown here. **d**, The set of individual a_{cyl} measurements are fitted to the cumulative distribution function of a normal distribution with mean μ and standard deviation σ. N is the number of individual measurements. This least-squares fit (solid black line) gives a_{cyl} for the dataset.

densities. A sharp transition away from the symmetric, uncoupled phase will occur only in a vacuum chamber larger than π/μ, and forces are suppressed at distances much smaller than $1/\mu$, so the range[10,11] of μ probed by our experiment is approximately $0.01\,\mathrm{meV} < \mu < 1\,\mathrm{meV}$.

Our basic set-up has been described previously[9]. To reach the sensitivity to observe the gravitational attraction between the atoms and the source mass, we installed significant technical upgrades. Three-dimensional Raman sideband cooling reduces the atom temperature to ∼300 nK. Launching the atoms vertically upwards in a cavity-enhanced optical lattice doubles the available interrogation time and quadruples the accumulated phase. Two levels of passive vibration isolation attenuate seismic noise, and an active stabilization loop provides further attenuation. After the interferometer, performing the lattice launch in reverse 'catches' atoms remaining in the cavity mode while the rest fall away. This spatial selection of atoms participating in the interferometer increases contrast by an order of magnitude to over 40%.

A schematic of our apparatus is shown in Fig. 1. Laser beams inside a Fabry–Pérot cavity provide well-controlled optical wavefronts and resonant power enhancement for coherent manipulation of the atomic probe. A tungsten cylinder of mass $m_{cyl} = 0.19\,\mathrm{kg}$ is our source mass. We have optimized this geometry using detailed numerical calculations of screened field profiles[22] in our vacuum chamber. An axial through-hole allows the cavity mode to pass through the mass unimpeded. A rectangular slot along one side of the cylinder allows the mass to be toggled between one position near the atoms and another position far away, without interrupting the cavity mode. A differential measurement between the two positions suppresses the Earth's gravitational acceleration and isolates the acceleration arising from the cylindrical source mass, $a_{cyl} = a_{near} - a_{far}$. This acceleration should be purely gravitational in the absence of any anomalous interactions.

Data was taken for more than 170 h through three quiet weekends in October 2016, resulting in $\sim 4.3 \times 10^5$ experimental runs (see Fig. 2). Averaging the measurements of the acceleration a_{cyl} weighted by the standard error over these three datasets results in $a_{cyl} = (74 \pm 19_{stat} \pm 15_{syst})\,\mathrm{nm\,s^{-2}}$, where the first error bar (one standard deviation) is statistical and the second arises from systematic uncertainties (see Methods). The positive acceleration indicates a force toward the source mass. This agrees well with the expected gravitational pull of the cylinder $a_{grav} = (65 \pm 5)\,\mathrm{nm\,s^{-2}}$. We obtain an anomalous acceleration $a_{anomaly} = a_{cyl} - a_{grav} = (9 \pm 24)\,\mathrm{nm\,s^{-2}}$, giving a 95% confidence interval of $-39\,\mathrm{nm\,s^{-2}} < a_{anomaly} < 57\,\mathrm{nm\,s^{-2}}$. Using a one-tailed test to bound fifth force interactions (which must be attractive for scalar fields with a universal matter coupling), we constrain anomalous accelerations $a_{anomaly} < 49\,\mathrm{nm\,s^{-2}}$ at the 95% confidence level. We note that the $24\,\mathrm{nm\,s^{-2}}$ (1σ) accuracy required to resolve the gravity signature from our miniature mass corresponds to just 2.4 ppb in the Earth's acceleration of free fall. Although spatial constraints set by the miniature size of the mass preclude using the beam sizes, and free-fall distances used in the best absolute gravimeters[15,16], we can resolve such a small acceleration by toggling the mass position, thereby suppressing systematic effects.

Specializing to chameleon and symmetron fields, following Burrage *et al.*[8], we improve previous limits[9–11] on these models by more than two orders of magnitude. Figure 3 shows excluded parameter ranges for these models. For chameleon fields with Λ at the dark energy value $\Lambda_0 = 2.4\,\mathrm{meV}$ and $n = 1$, we exclude up to $M < 2.8 \times 10^{-3}\ M_{Pl}$, narrowing the gap to torsion pendulum constraints[1,27]. One can see that these fields are nearly ruled out, with

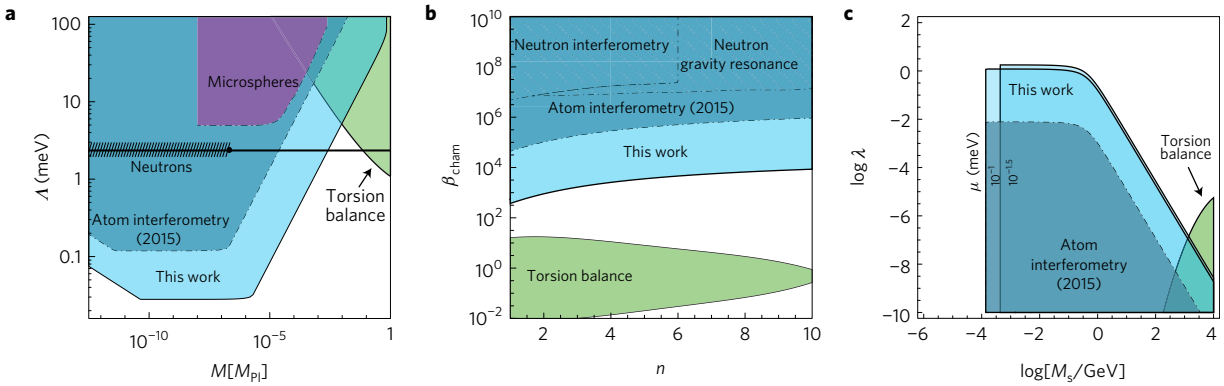

Figure 3 | Constraints on screened scalar fields. a, Chameleon field: the shaded areas in the M–Λ plane are ruled out at the 95% confidence level. M_{Pl}/M gives the coupling strength to normal matter in relation to gravity; $\Lambda = \Lambda_0 \approx 2.4$ meV (indicated by the black line) could drive cosmic acceleration today. A comparison is made to previous experiments: neutron interferometry[28]/neutron gravity resonance[29], microsphere force sensing[30], and torsion balance[1,27]. **b**, Chameleon limits in the n–β_{cham} plane with $\Lambda = \Lambda_0$, showing the narrowing gap in which basic chameleon theories could remain viable. n is the power law index describing the shape of the chameleon potential; $\beta_{cham} \equiv M_{Pl}/M$ is the strength of the matter coupling. **c**, Symmetron fields: constraints by atom interferometry complement those from torsion pendulum experiments[10,11] (shown with $\mu = 0.1$ meV) for the range of μ considered. For $\mu < 10^{-1.5}$ meV, the field vanishes entirely inside the vacuum (see Methods), leaving this parameter space unconstrained. The same effect produces the sharp cutoff in our limits at low M_S.

only a one order of magnitude range left for the coupling strength M. Furthermore, for all $\Lambda > 5.1$ meV, this gap is fully closed, ruling out all such models. Our symmetron limits are complementary to torsion pendula[1,10,11] as well. We improve previous constraints on λ by two orders of magnitude throughout the entire range of M_S and μ probed by our experiment. Our constraint is strongest in the regime where the atom is screened, where for $\mu = 0.1$ meV we rule out $\lambda < 1$.

Tests of gravity in the ultraweak-field regime with a miniature, in-vacuum source mass probe screened field theories with the potential to explain the accelerated expansion of our universe. In the future, technologies such as lattice interferometry[13] in our optical cavity and large momentum transfer Bragg beam splitters will allow us to hold quantum probe particles in proximity to a miniature source mass, evading geometric constraints from the source mass' small size, and boosting sensitivity. With modest improvements, chameleon fields at the cosmological energy density will be either discovered or completely ruled out. This also will enable study of novel quantum phenomena such as the gravitational Aharonov–Bohm effect[12], and provide even better resolution of atom–source mass interactions.

Methods

Methods, including statements of data availability and any associated accession codes and references, are available in the online version of this paper.

Received 24 January 2017; accepted 25 May 2017; published online 3 July 2017

References

1. Kapner, D. J. *et al*. Tests of the gravitational inverse-square law below the dark-energy length scale. *Phys. Rev. Lett.* **98,** 21101 (2007).
2. Colella, R., Overhauser, A. W. & Werner, S. A. Observation of gravitationally induced quantum interference. *Phys. Rev. Lett.* **34,** 1472–1474 (1975).
3. Peters, A., Chung, K. & Chu, S. Measurement of gravitational acceleration by dropping atoms. *Nature* **400,** 849–852 (1999).
4. Hornberger, K., Gerlich, S., Haslinger, P., Nimmrichter, S. & Arndt, M. Colloquium: quantum interference of clusters and molecules. *Rev. Mod. Phys.* **84,** 157–173 (2012).
5. Rosi, G., Sorrentino, F., Cacciapuoti, L., Prevedelli, M. & Tino, G. M. Precision measurement of the Newtonian gravitational constant using cold atoms. *Nature* **510,** 518–521 (2014).
6. Fixler, J. B., Foster, G. T., McGuirk, J. M. & Kasevich, M. A. Atom interferometer measurement of the newtonian constant of gravity. *Science* **315,** 74–77 (2007).
7. Arkani-Hamed, N. *et al*. The string landscape, black holes and gravity as the weakest force. *J. High Energy Phys.* **2007,** 060 (2007).
8. Burrage, C., Copeland, E. J. & Hinds, E. A. Probing dark energy with atom interferometry. *J. Cosmol. Astropart. Phys.* **2015,** 042 (2015).
9. Hamilton, P. *et al*. Atom-interferometry constraints on dark energy. *Science* **349,** 849–851 (2015).
10. Burrage, C., Kuribayashi-Coleman, A., Stevenson, J. & Thrussell, B. Constraining symmetron fields with atom interferometry. *J. Cosmol. Astropart. Phys.* **2016,** 041 (2016).
11. Brax, P. & Davis, A.-C. Atomic interferometry test of dark energy. *Phys. Rev. D* **94,** 104069 (2016).
12. Hohensee, M. A., Estey, B., Hamilton, P., Zeilinger, A. & Müller, H. Force-free gravitational redshift: proposed gravitational Aharonov–Bohm experiment. *Phys. Rev. Lett.* **108,** 230404 (2012).
13. Charrière, R., Cadoret, M., Zahzam, N., Bidel, Y. & Bresson, A. Local gravity measurement with the combination of atom interferometry and Bloch oscillations. *Phys. Rev. A* **85,** 13639 (2012).
14. Kovachy, T. *et al*. Quantum superposition at the half-metre scale. *Nature* **528,** 530–533 (2015).
15. Hu, Z.-K. *et al*. Demonstration of an ultrahigh-sensitivity atom-interferometry absolute gravimeter. *Phys. Rev. A* **88,** 43610 (2013).
16. Fang, B. *et al*. Metrology with atom interferometry: inertial sensors from laboratory to field applications. *J. Phys. Conf. Ser.* **723,** 12049 (2016).
17. Schmöle, J. *et al*. A micromechanical proof-of-principle experiment for measuring the gravitational force of milligram masses. *Class. Quantum Gravity* **33,** 125031 (2016).
18. Collaboration, P. Planck 2015 results. XIII. Cosmological parameters. *Astron. Astrophys.* **594,** A13 (2016).
19. Perlmutter, S. *et al*. Measurements of Ω and Λ from 42 high- redshift supernovae. *Astrophys. J.* **517,** 565–586 (1999).
20. Joyce, A., Jain, B., Khoury, J. & Trodden, M. Beyond the cosmological standard model. *Phys. Rep.* **568,** 1–98 (2015).
21. Will, C. M. The confrontation between general relativity and experiment. *Living Rev. Relat.* **17,** 4 (2014).
22. Elder, B. *et al*. Chameleon dark energy and atom interferometry. *Phys. Rev. D* **94,** 44051 (2016).
23. Brax, P., van de Bruck, C., Davis, A.-C., Khoury, J. & Weltman, A. Detecting dark energy in orbit: the cosmological chameleon. *Phys. Rev. D* **70,** 123518 (2004).
24. Khoury, J. & Weltman, A. Chameleon fields: awaiting surprises for tests of gravity in space. *Phys. Rev. Lett.* **93,** 171104 (2004).
25. Olive, K. A. & Pospelov, M. Environmental dependence of masses and coupling constants. *Phys. Rev. D* **77,** 43524 (2008).
26. Hinterbichler, K., Khoury, J., Levy, A. & Matas, A. Symmetron cosmology. *Phys. Rev. D* **84,** 103521 (2011).
27. Upadhye, A. Dark energy fifth forces in torsion pendulum experiments. *Phys. Rev. D* **86,** 102003 (2012).
28. Li, K. *et al*. Neutron limit on the strongly-coupled chameleon field. *Phys. Rev. D* **93,** 62001 (2016).

29. Jenke, T. *et al*. Gravity resonance spectroscopy constrains dark energy and dark matter scenarios. *Phys. Rev. Lett.* **112,** 151105 (2014).
30. Rider, A. D. *et al*. Search for screened interactions associated with dark energy below the 100 μm length scale. *Phys. Rev. Lett.* **117,** 101101 (2016).

Acknowledgements

We thank B. Estey for helpful discussions and technical contributions to the apparatus. This material is based upon work supported by the National Science Foundation under CAREER Grant No. PHY-1056620, the David and Lucile Packard Foundation, and National Aeronautics and Space Administration Grants No. 1553641, No. 1531033, and No. 1465360. We also acknowledge collaboration with Honeywell Aerospace under DARPA Contract No. N66001-12-1-4232. P.Haslinger thanks the Austrian Science Fund (FWF): J3680. B.E. and J.K. are supported in part by NSF CAREER Award PHY-1145525, NASA ATP grant NNX11AI95G, and the Charles E. Kaufman Foundation of the Pittsburgh Foundation.

Author contributions

M.J., P.Haslinger, V.X., P.Hamilton and H.M. built the apparatus, took the measurements, and performed the data analysis. B.E. performed numerical simulations of screened fields. A.U., B.E. and J.K. interpreted the measurements in the context of screened fields. All authors contributed to the manuscript.

Additional information

Supplementary information is available in the online version of the paper. Reprints and permissions information is available online at www.nature.com/reprints. Publisher's note: Springer Nature remains neutral with regard to jurisdictional claims in published maps and institutional affiliations. Correspondence and requests for materials should be addressed to H.M.

Competing financial interests

The authors declare no competing financial interests.

Methods

Setup. Here, we describe the basic outline and new features of our set-up[9,31]. Caesium atoms are loaded into a three-dimensional magneto-optical trap (3D-MOT) from a 2D-MOT. After sub-Doppler cooling in an optical molasses, we perform Raman sideband cooling[32] in a 3D lattice which leaves $\sim 5 \times 10^6$ atoms in the $|F=3, m_F=3\rangle$ state at a temperature <300 nK. After release from the lattice, adiabatic rapid passage and a state selection pulse with microwaves transfer the cold atoms into the magnetically insensitive $|F=3, m_F=0\rangle$ state. About 20% of the atoms are then launched upwards with a chirped optical lattice[13] in the optical cavity mode at a velocity of 59.1 cm s^{-1}. Launching the atoms moves them upwards towards the source mass, doubles the available interrogation time, and provides both spatial and velocity selection. After the launch, we perform the interferometry pulse sequence. The cavity dictates that all beams counter-propagate. Close to the apex, the Doppler shift δ_{Dopp} due to atom motion is small. The frequencies driving Raman transitions imparting upward momentum (k^+) therefore become degenerate with the ones imparting downward momentum (k^-). Since this would cause atom loss, we make our interferometer asymmetric with respect to the apex of the atomic trajectory. To increase signal to noise, we preferentially detect atoms at the centre of the Raman beam, suppressing the signal from atoms that have not participated in the interferometer. To this end, after the interferometer we reverse the launch procedure to catch the atoms by decelerating them into a lattice at zero velocity. This selects only the atoms in the centre of the cavity mode, while nonparticipating atoms (for example, that have left the cavity mode due to thermal expansion) fall away. A pushing beam separates the two output ports of the interferometer, where they are counted by fluorescence detection to determine their relative population.

Error budget. We discuss and quantify sources of uncertainty in the Supplementary Information. Systematic uncertainties for the individual datasets are combined, weighted by the statistical uncertainties of the datasets. Supplementary Table 1 shows the resulting error budget.

Vibration isolation. Vibrations of the retroreflecting cavity mirrors are a leading noise source. We mount the entire vacuum chamber on two layers of passive vibration isolation: a pneumatic benchtop isolation system (Thorlabs PWA 090), which is mounted on top of a floated optical table. For active isolation, a seismometer (Kinemetrics, SS-1) sits on top of the vacuum chamber to measure residual vibrations. The seismometer signal enters an analog feedback loop which actively stabilizes against vibrations using a voice coil actuator. The seismometer is magnetically shielded from switching experimental magnetic fields with a cylindrical pipe of low-carbon steel, reducing synchronous accelerations induced by the servo loop.

The passive isolation attenuates ground vibrations by up to two orders of magnitude. Closing the servo loop reduces the seismometer error signal a further factor of $\sim$5–400 from 1–20 Hz, the most problematic frequency range for our $2T = 110$ ms interferometer. This active servo loop reduces the expected interferometer phase noise by a factor of 16.

Numerical simulations. Computing the force from the scalar field on the atom involves solving equation (5), a nonlinear Poisson equation, for a matter distribution $\rho_{\mathrm{m}}(\mathbf{x})$ that corresponds to the experimental set-up. This includes the source mass, as well as the walls of the vacuum chamber. We do not compute the contribution from the atoms themselves in the calculation of φ; this effect is captured by the screening factor λ_{a}.

Our approach is to use a Gauss–Seidel finite-difference relaxation scheme on a three-dimensional grid that covers the entire experiment. An initial guess for the field inside the vacuum chamber is iteratively corrected until the field value converges everywhere. We have previously used this technique in the context of chameleons[22], which we have repeated for the new chameleon constraints and also extended to symmetrons. Once the field profile is known, equation (1) can be used to calculate the acceleration. We compute the average acceleration due to the scalar field as a time-weighted average over the trajectory of the atoms during the measurement.

Since the calculation is being done in near-vacuum, it is reasonable to expect the field profile to be roughly independent of M (for the chameleon) and M_{S} (for the symmetron). This is because those parameters only appear in their equation of motion along with ρ_{m}, which is very small. Supplementary Fig. 5a demonstrates this for the chameleon field, showing that the field's gradient is unchanged over five orders of magnitude in M.

Similarly, the vacuum value of φ for the symmetron field is inversely proportional to the square root of λ, so we might expect $\sqrt{\lambda}\varphi$ to be independent of λ. Indeed, Supplementary Fig. 5b shows $\lambda\varphi\nabla\varphi$ to be independent of both M_{S} and λ over six and ten orders of magnitude, respectively. This finding greatly expedites the numerics, as only a single simulation need be performed for a given value of μ.

As with refs 10,11, we find a measurable acceleration only for a relatively narrow range of μ: roughly $10^{-1.5}\,\mathrm{meV} < \mu < 10^{-1}\,\mathrm{meV}$. In fact, the lower end of our range in μ is an order of magnitude higher than that of ref. 10. This is because our 3D numerical code more accurately accounts for the presence of the vacuum chamber walls, which generically causes the field to vanish below a certain value of μ (or M_{S}, as seen in Fig. 3c). The upper end of μ is unchanged, and is due to the symmetron field becoming too short-ranged for the atoms to feel any appreciable force from the source mass.

Data availability. The data that support the plots within this paper and other findings of this study are available from the corresponding author upon reasonable request.

References

31. Hamilton, P. *et al*. Atom interferometry in an optical cavity. *Phys. Rev. Lett.* **114,** 100405 (2015).
32. Vuletić, V., Chin, C., Kerman, A. J. & Chu, S. Degenerate Raman sideband cooling of trapped cesium atoms at very high atomic densities. *Phys. Rev. Lett.* **81,** 5768–5771 (1998).